Hydrodynamics at the Navier-Stokes level applied to fast, transient, supersonic granular flows

Lidia Almazán, Clara Salueña, Vicente Garzó, José A. Carrillo, and Thorsten Pöschel

Citation: AIP Conf. Proc. **1501**, 993 (2012); doi: 10.1063/1.4769650
View online: http://dx.doi.org/10.1063/1.4769650
View Table of Contents: http://proceedings.aip.org/dbt/dbt.jsp?KEY=APCPCS&Volume=1501&Issue=1
Published by the American Institute of Physics.

Hydrodynamics at the Navier-Stokes Level Applied to Fast, Transient, Supersonic Granular Flows

Lidia Almazán[*], Clara Salueña[†], Vicente Garzó[**], José A. Carrillo[‡] and Thorsten Pöschel[*]

[*]*Institute for Multiscale Simulation, Universität Erlangen-Nürnberg, D-91052 Erlangen, Germany*
[†]*Departament d'Enginyeria Mecànica, Universitat Rovira i Virgili, 43007 Tarragona, Spain*
[**]*Departamento de Física, Universidad de Extremadura, E-06071 Badajoz, Spain*
[‡]*Department of Mathematics, Imperial College London, London SW7 2AZ, UK*

Abstract. We perform two-dimensional hydrodynamic simulations on a paradigmatic problem of granular dynamics, the Faraday instability, using two different approximations to the Navier-Stokes granular equations: the constitutive equations and kinetic coefficients derived from the assumption of vanishing inelasticity (Jenkins-Richman approach) obtained by solving the Enskog equation disks by means of Grad's method, and the ones obtained by solving the Enskog equation with the Chapman-Enskog method (Garzó-Dufty-Lutsko approach). The comparison reveals important qualitative and quantitative differences with respect to the hydrodynamic fields obtained by averaging results from particle simulations of the same system.

Keywords: rapid granular flows, Faraday instability, hydrodynamic simulations, molecular dynamics
PACS: 45.70.Qj, 45.70.Vn, 47.57.Gc

INTRODUCTION

The hydrodynamic modeling of granular materials has been a subject of interest for decades. To this development, particle simulations have contributed enormously. Thanks to all these efforts now there is a reasonable understanding of the granular gas, that is, a sufficiently dilute granular medium, under the idealizations that make the kinetic-theoretical treatment possible. Another question is the modeling of realistically dense material, of the type encountered as soon as one switches on gravity, for instance. The world of industrial applications is full of such examples. Dense flow of material particles has been largely modeled by means of molecular dynamics simulations, but the details of granular transport in this limit are not yet sufficiently understood.

The present contribution tries to add knowledge in this particular line. In dense granular flow often a huge number of particles is involved, making the listing of the collisional details of the number of encounters implied quite an expensive job –in terms of computer time and resources. A continuum description would be prefereable, however the hydrodynamic limit presents many questions, due to the failure of basic kinetic theory assumptions which generally occur when dealing with such systems (detailed balance, molecular chaos). However the most widely used hydrodynamic description for granular flow problems is the Navier-Stokes set of transport equations obtained from kinetic theory expansions, supplied with the corresponding constitutive equations along with their kinetic coefficients. Our aim here is to adopt the Navier-Stokes (NS) level of description, and compare the result from Computational Fluid Dynamics simulations with the Molecular Dynamics (MD) simulations of the same system.

For this purpose we select a paradigmatic problem of granular dynamics, intensively studied for the last two decades both experimentally and theoretically: the Faraday instability. The Faraday instability was described by Faraday in an appendix to an article in 1831. This instability consists in nonlinear stationary waves, as we can see in figure 1, that appear in a fluid within a container vibrated at a frequency that exceeds a critical value in presence of gravity. The onset of the Faraday waves, as well as its espatial and temporal periodicity, has been observed and studied in granular materials in [1, 2, 3, 4, 5]. Theoretical models have also been made in [6, 7].

Note that the choice of this problem poses important challenges: the formation of Faraday waves is a problem with strong time dependent evolution, plus transient shock waves propagating through the system, plus the development of a hydrodynamic instability, all this through a few layers of grains. In some sense, a problem like this pushes the NS hydrodynamics to the limit: Knudsen effects, strong shocks, lack of scale separation. Still, the ability of NS hydrodynamics applied to this system is remarkable, as we showed in [8] using the Jenkins-Richman [9] set of NS equations, however the quantitative comparison with MD is not perfect and shows a discrepancy of about 20%, Now

28th International Symposium on Rarefied Gas Dynamics 2012
AIP Conf. Proc. 1501, 993-1000 (2012); doi: 10.1063/1.4769650

we want to find out whether the use of a more appropriate model for inelastic grains [10, 11, 12] is capable to reduce this discrepancy, and test the adequacy of the Navier-Stokes description to this problem.

THE NAVIER-STOKES THEORY

We consider a granular fluid composed of smooth inelastic hard disks of mass m and diameter σ. Collisions are characterized by a (constant) coefficient of normal restitution $0 < \alpha \leq 1$. Starting from the (inelastic) Enskog kinetic equation [13, 14], one can easily obtain the Navier-Stokes hydrodynamic equations for the number density $n(\vec{r},t)$, the flow velocity $\vec{u}(\vec{r},t)$, and the local temperature $T(\vec{r},t)$ [15]

$$\frac{\partial n}{\partial t} + \vec{\nabla}\cdot(n\vec{u}) = 0\,, \tag{1}$$

$$\rho\left(\frac{\partial \vec{u}}{\partial t} + \vec{u}\cdot\vec{\nabla}\vec{u}\right) = -\vec{\nabla}\cdot\hat{P} + n\vec{F}\,, \tag{2}$$

and

$$n\left(\frac{\partial T}{\partial t} + \vec{u}\cdot\vec{\nabla}T\right) = -\nabla\cdot\vec{q} - \hat{P}:\vec{\nabla}\vec{u} - \zeta nT\,. \tag{3}$$

In the above equations, $\rho = mn$ is the mass density, $\vec{F}$ is the external force acting on the system, $\hat{P}$ is the pressure tensor, $\vec{q}$ is the heat flux, and ζ is the cooling rate due to the energy dissipated in collisions. The constitutive equations which define the momentum and heat fluxes $\hat{P}$, $\vec{q}$, which depend in general on the coefficient of restitution α, must be specified in terms of the hydrodynamic fields and their spatial gradients. To first order in the spatial gradients, the Navier-Stokes constitutive equations provide a closure for the hydrodynamic fields. The constitutive relation of the pressure tensor P_{ij} is

$$P_{ij} = p\delta_{ij} - \eta\left(\partial_j u_i + \partial_i u_j - \delta_{ij}\vec{\nabla}\cdot\vec{u}\right) - \gamma\delta_{ij}\vec{\nabla}\cdot\vec{u}, \tag{4}$$

where p is the hydrostatic pressure, η is the shear viscosity, and γ is the bulk viscosity. The constitutive equation for the heat flux is

$$\vec{q} = -\kappa\vec{\nabla}T - \mu\vec{\nabla}n, \tag{5}$$

where κ is the coefficient of thermal conductivity, and μ is a new coefficient which does not have an analogue for a gas of elastic particles. Finally, to first order in gradients, the cooling rate ζ can be written as [13]

$$\zeta = \zeta_0 + \zeta_1\nabla\cdot\vec{u}\,. \tag{6}$$

The evaluation of the explicit form of the hydrostatic pressure p, the Navier-Stokes transport coefficients η, γ, κ, and μ and the coefficients ζ_0 and ζ_1 requires to solve the corresponding Enskog equation. However, due to its complexity, only approximate results for the above coefficients can be obtained. Here, we consider two independent approaches for hard disks proposed by Jenkins and Richman [9] and Garzó and Dufty [10] and Lutsko [12].

Jenkins-Richman (JR) Approach

The results derived by Jenkins and Richman [16, 9] are obtained by solving the Enskog equation for spheres [16] and disks [9] by means of Grad's method [17]. The expansion of the velocity distribution function in terms of generalized Hermite polynomials is truncated and substituted into the hierarchy of moment equations, providing a closed set of coupled equations for the hydrodynamic fields (n, $\vec{u}$, and T) plus the irreversible momentum and heat fluxes ($P_{ij} - p\delta_{ij}$ and $\vec{q}$).

The explicit forms of the hydrostatic pressure, the Navier-Stokes transport coefficients and the cooling rate in the JR theory are given by

$$p_{\rm JR} = \frac{4}{\pi\sigma^2}\phi T[1+(1+\alpha)G(\phi)], \quad \eta_{\rm JR} = \frac{\phi}{2\sigma}\sqrt{\frac{mT}{\pi}}\left[\frac{1}{G(\phi)} + 2 + \left(1+\frac{8}{\pi}\right)G(\phi)\right], \quad \gamma_{\rm JR} = \frac{8}{\pi\sigma}\phi G(\phi)\sqrt{\frac{mT}{\pi}}\,, \tag{7}$$

$$\kappa_{\rm JR} = \frac{2\phi}{\sigma}\sqrt{\frac{T}{\pi m}}\left[\frac{1}{G(\phi)} + 3 + \left(\frac{9}{4}+\frac{4}{\pi}\right)G(\phi)\right], \quad \mu_{\rm JR} = 0,$$
$$\zeta_{0,\rm JR} = \frac{4}{\sigma}(1-\alpha^2)\sqrt{\frac{T}{\pi m}}G(\phi), \qquad \zeta_{1,\rm JR} = 0. \tag{8}$$

In the above equations, $\phi = n\pi\sigma^2/4$ is the (dimensionless) volume fraction occupied by the granular disks, also called packing fraction, $G(\phi) = \phi\chi(\phi)$, and $\chi(\phi)$ is the pair correlation function.

The results derived by Jenkins and Richman [9] neglect the cooling effects on temperature due to the cooling rate in the expressions of the transport coefficients, assumption which can only be considered as acceptable for nearly elastic systems ($\alpha \to 1$). As a consequence, the coefficient of restitution α only enters in the equation of state (7) and in the expression (8) for the zeroth-order cooling rate ζ_0. Therefore the expressions of the Navier-Stokes transport coefficients $\eta_{\rm JR}$, $\gamma_{\rm JR}$, and $\kappa_{\rm JR}$ are the same as those given by the Enskog equation for elastic disks [18].

In order to get the dependence of the transport coefficients and the cooling rate in both JR and GDL approaches, one has to choose an approximate form for the pair correlation function $\chi(\phi)$. In this paper, we have chosen the form proposed by Torquato [19],

$$\chi(\phi) = \begin{cases} \dfrac{1-\frac{7}{16}\phi}{(1-\phi)^2} & \text{for } 0 \le \phi < \phi_f, \\ \dfrac{1-\frac{7}{16}\phi_f}{(1-\phi_f)^2}\dfrac{\phi_c-\phi_f}{\phi_c-\phi} & \text{for } \phi_f \le \phi \le \phi_c, \end{cases} \tag{9}$$

which goes through the freezing point $\phi_f = 0.69$ and approaches reasonably the random close packing limit, $\phi_c = 0.82$.

Garzó-Dufty-Lutsko Approach

The dependence of the Navier-Stokes transport coefficients on the coefficient of restitution was first obtained by Garzó and Dufty [10] for hard spheres ($d = 3$) by solving the Enskog equation from the Chapman-Enskog method [11]. These results were then extended to an arbitrary number of dimensions by Lutsko [12]. Here, we refer to the above theories as the GDL theory. The main difference with respect to the JR approach is that these results are not limited to weak inelasticity since they incorporate the complete nonlinear dependence on α. In the following we summarize the results of the Navier-Stokes transport coefficients and equation of state for hard disks,

$$p_{\rm GDL} = p_{\rm JR} = \frac{4}{\pi\sigma^2}\phi T[1 + (1+\alpha)G(\phi)], \tag{10}$$

$$\gamma_{\rm GDL} = \frac{4}{\pi\sigma}\phi G(\phi)\sqrt{\frac{mT}{\pi}}(1+\alpha)\left(1-\frac{c}{32}\right), \tag{11}$$

$$\eta_{\rm GDL} = \frac{\sqrt{mT/\pi}}{2\sigma}\frac{\left[1-\frac{1}{4}(1+\alpha)(1-3\alpha)G(\phi)\right]\left[1+\frac{1}{2}G(\phi)(1+\alpha)\right]}{\nu_\eta^* - \frac{1}{2}\zeta_0^*} + \frac{1}{2}\gamma_{\rm GDL}, \tag{12}$$

$$\kappa_{\rm GDL} = \frac{2}{\sigma}\sqrt{\frac{T}{\pi m}}\left\{\left[1+\frac{3}{4}G(\phi)(1+\alpha)\right]\kappa_k^* + \frac{2}{\pi}\phi G(\phi)(1+\alpha)\left(1+\frac{7c}{32}\right)\right\}, \tag{13}$$

$$\mu_{\rm GDL} = \frac{T\sigma}{\phi}\sqrt{\frac{\pi T}{m}}\left[1+\frac{3}{4}G(\phi)(1+\alpha)\right]\mu_k^* \tag{14}$$

where the (reduced) kinetic contributions κ_k^* and μ_k^* are

$$\kappa_k^* = \frac{1+c+\frac{3}{8}G(\phi)(1+\alpha)^2\left[2\alpha-1+\frac{c}{2}(1+\alpha)\right]}{2(\nu_\kappa^* - 2\zeta_0^*)}, \tag{15}$$

$$\mu_k^* = \frac{\zeta_0^*\kappa_k^*(1+\phi\partial_\phi\ln\chi) + \frac{c}{4} + \frac{3}{8}G(\phi)(1+\alpha)(1+\frac{1}{2}\phi\partial_\phi\ln\chi)\left[\alpha(\alpha-1)+\frac{c}{12}(14-3\alpha+3\alpha^2)\right]}{2\nu_\kappa^* - 3\zeta_0^*}. \tag{16}$$

In (12)–(16) we have introduced the quantities [20]

$$\zeta_0^* = \frac{1}{2}\chi(\phi)(1-\alpha^2)\left(1+\frac{3c}{32}\right), \tag{17}$$

$$\nu_\eta^* = \frac{1}{8}\chi(\phi)(7-3\alpha)(1+\alpha)\left(1+\frac{7c}{32}\right), \tag{18}$$

$$\nu_\kappa^* = \frac{1}{4}\chi(\phi)(1+\alpha)\left[1+\frac{15}{4}(1-\alpha)+\frac{365-273\alpha}{128}c\right], \tag{19}$$

where

$$c(\alpha) = \frac{32(1-\alpha)(1-2\alpha^2)}{57-25\alpha+30\alpha^2(1-\alpha)}\,. \tag{20}$$

Also taking into account (9), we obtain the expression

$$\frac{\partial}{\partial\phi}\ln\chi(\phi) = \begin{cases} \dfrac{25-7\phi}{(16-7\phi)(1-\phi)} & \text{for } 0 \le \phi < \phi_f \\ \dfrac{1}{(\phi_c-\phi)} & \text{for } \phi_f \le \phi < \phi_c \end{cases}, \tag{21}$$

to be used in (16).

More details can be found in [21]. Note that the expressions derived by Lutsko [12] neglect in the expressions (18) and (19) of ν_η^* and ν_κ^*, respectively, the factors of c coming from the non-Gaussian corrections to the reference state. These extra factors will be accounted for in our numerical results since their effect on transport becomes non negligible at small values of α. Finally, the contributions to the cooling rate are given by

$$\zeta_{0,\mathrm{GDL}} = \frac{4}{\sigma}(1-\alpha^2)\sqrt{\frac{T}{\pi}}G(\phi)\left(1+\frac{3c}{32}\right), \tag{22}$$

$$\zeta_{1,\mathrm{GDL}} = \frac{3}{2}G(\phi)(1-\alpha^2)\left[\frac{3}{32}\frac{\frac{1}{8}\omega^* - c(1+\alpha)(\frac{1}{3}-\alpha)}{\nu_\zeta^* - \frac{3}{4}(1-\alpha^2)} - 1\right], \tag{23}$$

where

$$\nu_\zeta^* = -\frac{1+\alpha}{192}(30\alpha^3-30\alpha^2+153\alpha-185), \tag{24}$$

$$\omega^* = (1+\alpha)\left[(1-\alpha^2)(5\alpha-1) - \frac{c}{12}(15\alpha^3-3\alpha^2+69\alpha-41)\right]. \tag{25}$$

NUMERICAL SCHEME

We refer to [8] for the full details of the numerical scheme that here is applied to both the GDL and the JR Navier-Stokes hydrodynamic equations since they share the same structure. Briefly, the Navier-Stokes terms are treated by simple centered high-order explicit in time finite difference approximations and considered as sources for the method of lines in the time approximation. Meanwhile the Euler (convective) terms are solved in local coordinates by a fifth-order explicit in time finite difference characteristic-wise WENO method in a uniform grid following [22, 23]. This scheme guarantees a monotonous propagation of sharp shock-wave fronts with small diffusion. The top and bottom walls in both hydrodynamic simulations are adiabatic and impenetrable. More precisely, the normal velocity is zero at the walls, the energy flux is zero, and the tangential velocity remains unchanged. The simulation is carried over in the comoving frame of the wall, and thus the force per unit mass of the simulated system is $\vec{F} = (-g + A\sin(2\pi f t))\vec{j}$, with $\vec{j} = (0,1)$.

As for the MD simulations, we follow a traditional approach as in [8]. In MD as well as when solving the 2D-Navier-Stokes equations, we fix the frequency of the piston motion $f = 3.75$ Hz, and the amplitude $A = 5.6$ particle diameters. The system size is tuned to fit three pattern wavelengths in the (horizontal) x-direction ($125\,\sigma$), which is periodic. Except for the MD system, which is not limited vertically, the y-direction is constrained to $60\,\sigma$, which ensures that the packing fraction at the top wall is not larger than ≈ 0.001. The particles are 783 disks of diameter $\sigma = 1$ cm and mass $m = 1$ mg, and $g = 9.81$ m/s^2 is the acceleration of gravity.

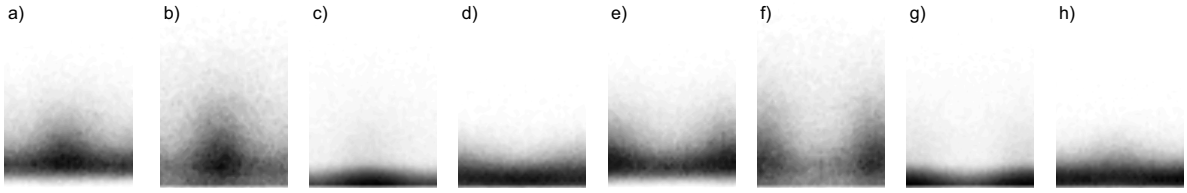

FIGURE 1. Density field obtained by phase- and space-averaging particle positions from the MD simulation, around one of the peaks/valleys characteristic of the granular Faraday instability. Subfigures (a) to (h) show the time evolution through a window frame which covers a single wavelength. To get the view of the entire pattern, just imagine a periodic copy of each one of these eight snapshots along the horizontal direction.

RESULTS AND DISCUSSION

The MD results are phase- and space- averaged following a procedure which has been explained in detail in [8]. The results are 2D-hydrodynamic fields which can be compared with the corresponding JR and GDL fields in any two consecutive cicles, once the typical biperiodic Faraday waves characteristic of this instability have fully developed.

In figures 2-6, from top to bottom, we show the packing fraction, temperature, internal energy, kinetic energy and heat flow profiles, plotted on the x-axis at the location occupied by a peak (and a valley, alternatively). While the hydrodynamic fields are two dimensional (see figure 1) , we will show a 1D reduction for a better understanding and presentation. Moreover, the selected position shows the largest changes which can be observed in the system and what happens there is representative of the entire 2D domain. In the following plots, the vertical axis is height, and the subfigures (a-h) correspond to the times $t = 0$; $^1/_4\tau$; $^2/_4\tau$; ...; $^7/_4\tau$, where $\tau = f^{-1}$.

At time $t = 0$ (a), the piston is going down through the equilibrium position; between (a) and (c), we see the growth and the dissolution of the central peak (the position of which is taken as the reference for the one-dimensional profiles shown below). The height of the material in (a) is growing to a maximum, clearly seen in (b). Shortly after (a), the granular layer experiences the impact against the bottom wall and the propagation of a shock wave. Just instants following frame (c), the layer becomes flat –so does after frame (g), and the material floods to neighboring positions to create peaks where valleys previously existed. Shortly after (e), another impact with the plate takes place. From frame (d) to frame (g), we see the evolution of the density at a valley.

The most striking difference between the GDL and JR solutions is the temperature field (see figure 3). At large heights, the GDL temperature is one order of magnitude larger than the JR. Moreover, the GDL temperature gradient is positive at middle heights whereas there the JR, like the MD temperature gradient, is negative once the shock wave is dissipated. It is the term $\mu\nabla n$ in the heat flux (5) which helps to sustain large temperature gradients in the system, transferring heat from the dense to the dilute regions at the top wall. This term, which vanishes in the JR approach ($\mu_{JR} = 0$), is a genuine contribution of the inelastic nature of the granular gas to the transport coefficients. However we find no hint in the obtained MD profile that the temperature gradient should be positive instead of negative when ascending from the dense to the dilute region.

In figure 6 we show the vertical component of the heat flux as a function of height. Unlike the JR, the GDL heat flux consists of two terms, the one coming from the temperature gradient, and the one associated, through the coefficient μ, to the density gradient. The role of the latter contribution is to transfer heat from the dense towards the dilute regions at the top, while the former brings energy into the granulate, from the high temperature regions at the top. Both terms are relevant and contribute in the same order of magnitude, although an analysis reveals that they have generally opposite signs. So, the heat transfer dynamics is quite different in the GDL and the JR approaches, in such a way that gives rise to entirely different solutions for the temperature field. The comparison of the internal energy profiles (see figure 4) reinforces the quite unexpected result that the GDL solution is not closer to the MD, but even further away, than the JR.

The scaled kinetic energy profiles are shown in figure 5. The differences show that the GDL solution for the velocity field is also quantitatively different from the JR, a consequence of the inelasticity contributing to the viscosities. The acute drops at intermediate heights signal the changes of sign of the vertical velocity. These occur at different times, due to the delayed landing of the granular layer in the MD simulation. In this case, however, the decay of the kinetic energy at large heights is qualitatively and quantitatively quite well reproduced, in the JR as well as in the GDL

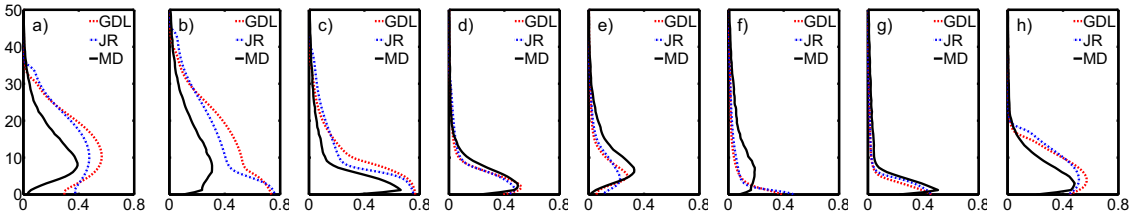

FIGURE 2. On the x-axis, the packing fraction; here and in the following profiles the y-axis is the height in diameters (σ).

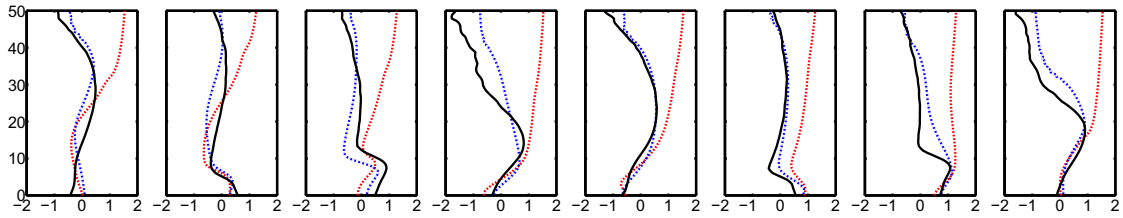

FIGURE 3. On the horizontal axis, $\log_{10}$ of the adimensional temperature, $T/(g\sigma)$.

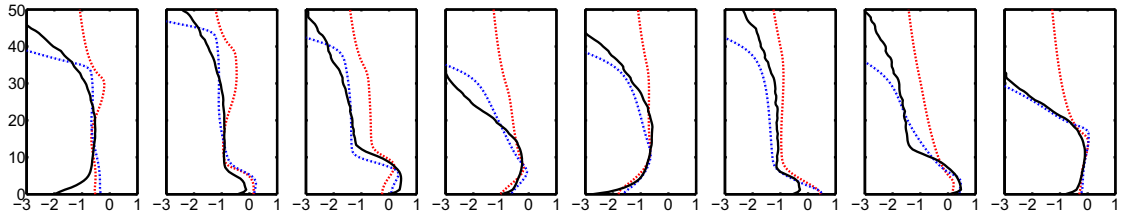

FIGURE 4. On the horizontal axis, $\log_{10}$ of the scaled internal energy, $\phi T/(g\sigma)$

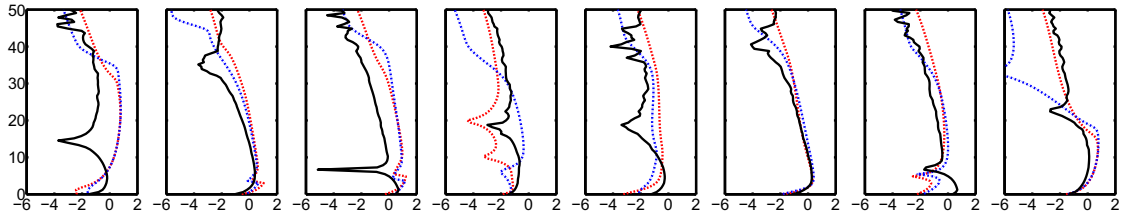

FIGURE 5. On the horizontal axis, $\log_{10}$ of the scaled kinetic energy, $\phi u^2/(2g\sigma)$

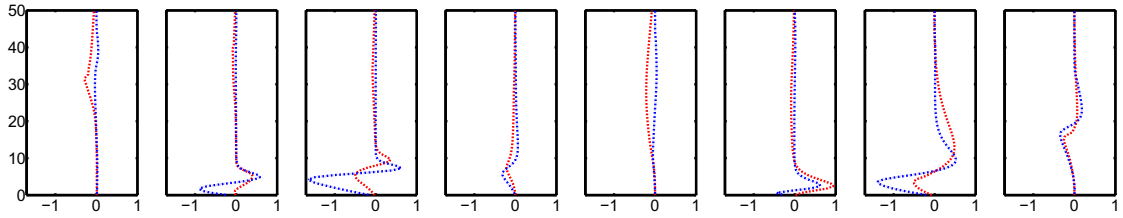

FIGURE 6. On the horizontal axis, vertical component of the reduced heat flux $q_y/(g\sqrt{\sigma g})$

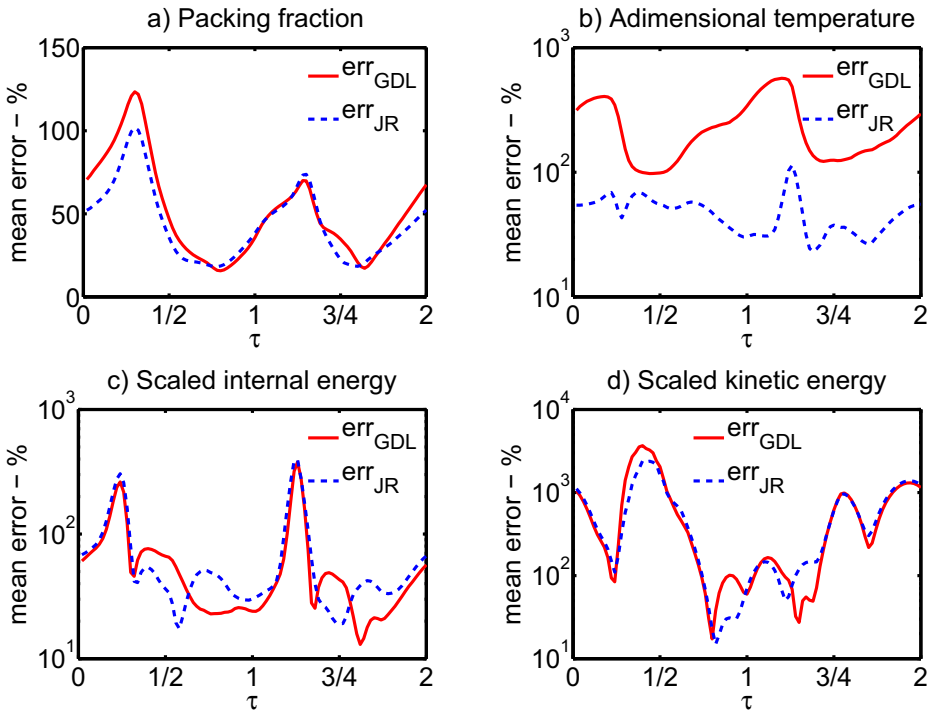

FIGURE 7. Root-mean-square error of the JR and GDL results, in percentages, computed trhough two consecutive periods with respect to the MD results for the profiles studied.

simulations.

The disagreement of the JR and GDL profiles with respect to the MD can be quantified through a root-mean-square error $\sqrt{\langle(\psi-\psi_{MD})^2\rangle/\langle\psi_{MD}^2\rangle}$, where ψ is any of the hydrodynamic variables (packing fraction, temperature, internal energy and kinetic energy) in the JR or GDL approaches, with the average being taken over the entire height and using ϕ_{MD} (the packing fraction obtained from MD) as a weight function –in order to account for discrepancies only in regions where particles are effectively present. The results, as a function of time over the two cycles, are represented in figure 7. Even if the discrepancies seem large, we remark that they include the effect of the early landing of the granular layer in the JR and GDL simulations, which advances the propagation of the shock wave giving rise to entirely different profiles to those obtained from MD at the same times. Thus, in some stages the MD profiles are delayed by 0.16τ with respect to the JR and GDL (see this effect in the periodic growth of the error in figure 7), but instead the errors add up without reflecting the time correlation between frames which actually exists.

From these results, one has to conclude that the granular Navier-Stokes hydrodynamics with the proper GDL forms for the transport coefficients is not capable of reducing the discrepancy between discrete particle simulations and hydrodynamic simulations of moderately dense, inelastic gases. Surprisingly, the discrepancies between theory and simulations decrease if one considers the elastic (JR) forms of the transport coefficients, which has no physical explanation. Far from making the JR a better choice, this fact rather signals the failure of the NS hydrodynamics to describe such a highly nonlinear problem. In fact the results point at the term $-\mu\nabla n$ in the heat flux as being responsible for the growth of the granular temperature at large heights. For this reason we can conclude that the transport coefficient μ is largely overestimated by the Navier-Stokes approximation and consequently, the influence of the diffusion term on the heat flux is much larger than the one observed in the MD simulations.

Finally, the quantitative disagreement must be attributed to the fact that the Navier-Stokes constitutive equations (4) and (5) for the pressure tensor and the heat flux, respectively only apply to first order in the spatial gradients, while the granular Faraday instability problem is outside the validity of the Navier-Stokes approximation as MD simulations clearly show.

ACKNOWLEDGMENTS

LA and JAC were partially supported by the project MTM2011-27739-C04-02 DGI (Spain) and 2009-SGR-345 from AGAUR-Generalitat de Catalunya. JAC acknowledges support from the Royal Society through a "Wolfson Research Merit Award". LA, JAC, and CS acknowledge support of the project Ingenio Mathematica FUT-C4-0175. CS and VG appreciate funding from the Spanish Ministry of Science and Innovation via the projects DPI2010-17212 and grant PR2008-0256 (CS) and FIS2010-16587 and grant GR10158 from the Junta de Extremadura (VG). LA and TP were supported by Deutsche Forschungsgemeinschaft through the Cluster of Excellence *Engineering of Advanced Materials*.

REFERENCES

1. H. K. Pak, and R. P. Behringer, *Phys. Rev. Lett.* **71**, 1832–1835 (1993).
2. F. Melo, P. Umbanhowar, and H. L. Swinney, *Phys. Rev. Lett.* **72**, 172–175 (1994).
3. F. Melo, P. B. Umbanhowar, and H. L. Swinney, *Phys. Rev. Lett.* **75**, 3838–3841 (1995).
4. P. B. Umbanhowar, F. Melo, and H. L. Swinney, *Nature* **382**, 793–796 (1996).
5. E. van Doorn, and R. Behringer, *Phys. Lett. A* **235**, 469–474 (1997), ISSN 0375-9601.
6. L. S. Tsimring, and I. S. Aranson, *Phys. Rev. Lett.* **79**, 213–216 (1997).
7. D. H. Rothman, *Phys. Rev. E* **57**, R1239–R1242 (1998).
8. J. A. Carrillo, T. Pöschel, and C. Salueña, *J. Fluid Mech.* **597**, 119–144 (2008).
9. J. Jenkins, and M. W. Richman, *Phys. Fluids* **28**, 3485–3494 (1985).
10. V. Garzó, and J. W. Dufty, *Phys. Rev. E* **59**, 5895–5911 (1999).
11. S. Chapman, and T. G. Cowling, *The Mathematical Theory of Nonuniform Gases.*, Cambridge University Press, London, 1970.
12. J. F. Lutsko, *Phys. Rev. E* **72**, 021306 (2005).
13. A. Goldshtein, and M. Shapiro, *J. Fluid Mech.* **282**, 75–114 (1995).
14. J. J. Brey, J. W. Dufty, and A. Santos, *J. Stat. Phys.* **87**, 1051–1066 (1997).
15. N. Brilliantov, and T. Pöschel, *Kinetic Theory of Granular Gases*, Oxford University Press, 2004.
16. J. Jenkins, and M. W. Richman, *Arch. Rational Mech. Anal.* **87**, 355–377 (1985).
17. H. Grad, *Comm. Pure Appl. Math.* **2**, 331–407 (1949).
18. D. M. Gass, *J. Chem. Phys.* **54**, 1898–1902 (1970).
19. S. Torquato, *Phys. Rev. E* **51**, 3170–3182 (1995).
20. V. Garzó, *arXiv:1204.5114* (2012).
21. L. Almazán, J. Carrillo, C. Salueña, V. Garzó, and T. Pöschel, *arXiv:1204.2415* (2012).
22. G. Jiang, and C.-W. Shu, *J. Comput. Phys.* **126**, 202–228 (1996).
23. C.-W. Shu, "Essentially non-oscillatory and weighted essentially non-oscillatory schemes for hyperbolic conservation laws," in *Advanced Numerical Approximation of Nonlinear Hyperbolic Equations*, edited by B. Cockburn, C. Johnson, C.-W. Shu, and E. Tadmor, Springer, Berlin, 1998, vol. 1697 of *Lecture Notes in Mathematics*, pp. 325–432.